

## A Mechanism and Simple Dynamical Model of the North Atlantic Oscillation and Annular Modes

GEOFFREY K. VALLIS, EDWIN P. GERBER, PAUL J. KUSHNER, AND BENJAMIN A. CASH

*Geophysical Fluid Dynamics Laboratory, Princeton University, Princeton, New Jersey*

(Manuscript received 27 February 2003, in final form 22 August 2003)

### ABSTRACT

A simple dynamical model is presented for the basic spatial and temporal structure of the large-scale modes of intraseasonal variability and associated variations in the zonal index. Such variability in the extratropical atmosphere is known to be represented by fairly well-defined patterns, and among the most prominent are the North Atlantic Oscillation (NAO) and a more zonally symmetric pattern known as an annular mode, which is most pronounced in the Southern Hemisphere. These patterns may be produced by the momentum fluxes associated with large-scale midlatitude stirring, such as that provided by baroclinic eddies. It is shown how such stirring, as represented by a simple stochastic forcing in a barotropic model, leads to a variability in the zonal flow via a variability in the eddy momentum flux convergence and to patterns similar to those observed. Typically, the leading modes of variability may be characterized as a mixture of “wobbles” in the zonal jet position and “pulses” in the zonal jet strength. If the stochastic forcing is statistically zonally uniform, then the resulting patterns of variability as represented by empirical orthogonal functions are almost zonally uniform and the pressure pattern is dipolar in the meridional direction, resembling an annular mode. If the forcing is enhanced in a zonally localized region, thus mimicking the effects of a storm track over the ocean, then the resulting variability pattern is zonally localized, resembling the North Atlantic Oscillation. This suggests that the North Atlantic Oscillation and annular modes are produced by the same mechanism and are manifestations of the same phenomenon.

The time scale of variability of the patterns is longer than the decorrelation time scale of the stochastic forcing, because of the temporal integration of the forcing by the equations of motion limited by the effects of nonlinear dynamics and friction. For reasonable parameters these produce a decorrelation time of the order of 5–10 days. The model also produces some long-term (100 days or longer) variability, without imposing such variability via the external parameters except insofar as it is contained in the nearly white stochastic forcing.

### 1. Introduction

The large-scale atmospheric circulation displays variability on multiple time scales. The most prominent variability in the extratropics is that due to baroclinic eddies, or midlatitude weather systems, which typically have a time scale of a few days. On time scales of a season or longer, atmospheric variability may be influenced by interactions at its boundaries (e.g., by the sea surface temperature) and by other slow changes in forcing. The variability on intermediate (i.e., intraseasonal) time scales, say between 10 days and a season (sometimes called “low-frequency” variability), has a less obvious cause. The direct effect of the ocean or other changing boundary seems unlikely to be important, both because large-scale sea surface temperatures tend to change primarily on still longer time scales and because

their effect is unlikely to be strong enough to produce large changes in the atmospheric circulation on the 10–100-day time scale. Rather, we expect this variability to have a primarily atmospheric origin, ultimately arising from baroclinic activity and weather systems and reddened by the dynamics of the equations of motion. The mechanisms of such variability, however, are not fully understood, and are the subject of this paper.

Although we may sometimes refer to intraseasonal variability as if there were a distinct time scale and a distinct phenomenon, there is no pronounced peak in the power spectrum of the atmospheric fields on the weeks-to-months time scale, nor is there a dip in the spectrum at time scales longer than that associated with baroclinic eddies. This suggests that the variability at intraseasonal time scales may be, at leading order, caused by a reddening of the power spectrum of the known forcing (i.e., baroclinic instability). That is, if we consider baroclinic instability to provide a nearly white stochastic forcing, then the barotropic response to such forcing will generally have a red spectrum. Both friction and nonlinear processes (i.e., chaos) tend to in-

---

*Corresponding author address:* Dr. Geoffrey K. Vallis, Atmospheric and Oceanic Sciences Program, Department of Geosciences, Princeton University, Princeton, NJ 08544-0710.  
E-mail: gkv@princeton.edu

hibit very long-term correlations and put a cap on the spectral reddening at some time scale, whitening the spectrum at long time scales and leading to decorrelation time scales potentially of about 10 days. (Whether fields in the real atmosphere also have significant autocorrelations on the multiyear or decadal time scale is not known, nor whether these could arise from a purely atmospheric origin.)

If the atmospheric fields are appropriately filtered in time to select intraseasonal time scales, then fairly well-defined spatial patterns of variability emerge. This spatial structure has been the object of much study and debate, going back at least as far as Walker and Bliss (1932), and summarized recently by Wallace (2000) and Wanner et al. (2002). The patterns robustly show up in correlation maps or teleconnection patterns (Wallace and Gutzler 1981), and in the empirical orthogonal functions (EOFs) of the low-passed fields (e.g., Ambaum et al. 2001), and a host of such patterns have been identified by these and other workers—the North Atlantic Oscillation (NAO), the Northern and Southern Annular Modes (NAM, SAM), the Pacific–North American pattern (PNA) and so on. Of these, the North Atlantic Oscillation is probably the most well known and this and the annular modes (Thompson and Wallace 2000) will mainly concern us in this paper. The scale of these patterns is significantly larger than that typically associated with a single baroclinic eddy, ranging from a few thousand kilometers of the NAO to the hemispheric scale of the annular modes. Two other aspects of their structure stand out: 1) they are barotropic, or at least equivalent barotropic (little phase shift in the vertical); 2) there is a strong dipolar component in the horizontal structure of the pressure field.

Although the patterns are of larger scale than baroclinic eddies, there is much to suggest that it is such eddy activity (i.e., weather systems) that is largely responsible for producing them, even though the patterns are fairly barotropic. On the theoretical side, large-scale eddy-driven structures often tend to be barotropic because the life cycle of baroclinic eddies is characterized by a barotropic decay and a cascade to larger horizontal and vertical scales (Rhines 1977; Simmons and Hoskins 1978; Salmon 1980). Idealized model simulations (e.g., Orlanski 1998) have also shown the important role of baroclinic eddies in producing the quasi-stationary circulation. On the observational side, analysis of annular modes and the NAO indicates that transient, high-frequency (i.e., 1–10 days) activity plays an important role in maintaining their variability (e.g., Lau 1988; Limpasuvan and Hartmann 2000; DeWeaver and Nigam 2000). Consistently, the midlatitude jet in the Atlantic sector is stronger during periods of high NAO index (Ambaum et al. 2001, their Figs. 6 and 7) and this jet is fairly barotropic, indicating an eddy-driven origin. Finally, recent experiments with a general circulation model (GCM; Cash et al. 2003, manuscript submitted to *J. Atmos. Sci.*, hereafter CKV) have shown a strong

correlation between the location and strength of the dipole with the location and strength of the baroclinic eddy activity.

Assuming, then, that the relevant large-scale dynamics are indeed barotropic, but that that eddy activity is important as the ultimate source of the variability, our goal now is to understand how such higher-frequency (1–10-day time scale) eddy dynamics can produce the characteristic spatial patterns seen on longer (10–50-day) time scales. Specifically, we seek to present a simple dynamical model, perhaps the simplest possible dynamical model, of the NAO and annular modes in order to shed insight on the dynamics of such structures. We shall not present a complete model or a complete theory. Rather, our model might be considered as a “dynamical null hypothesis” that might be built upon to create a more complete theory.

## 2. The basic model

### a. Jets on a $\beta$ plane

Consider first the maintenance of the extratropical jet. This has a different dynamical origin from the highly baroclinic subtropical jet. The latter arises from a thermal wind balance with the strong meridional temperature gradients at the edge of the Hadley cell, whereas the former is driven by eddy momentum flux convergence in midlatitude weather systems and, because these largely occur in the mature phase of the baroclinic life cycle, they act to produce a predominantly barotropic jet. In reality, the subtropical and midlatitude jets are often not geographically distinct because the polar limit of the Hadley cell overlaps the equatorial limit of the midlatitude baroclinic zone, and the jets may appear as one.

A simple barotropic model illustrates the mechanisms of the eddy driven jet (e.g., Held 2000). For two-dimensional incompressible flow, the barotropic zonal momentum equation is

$$\frac{\partial u}{\partial t} + u \frac{\partial u}{\partial x} + v \frac{\partial u}{\partial y} - fv = -\frac{\partial \phi}{\partial x} + F_u - D_u, \quad (2.1)$$

where  $F_u$  and  $D_u$  represent the effects of any forcing and dissipation and the other notation is standard. The meridional momentum and vorticity fluxes are related by the identity

$$v\zeta = \frac{1}{2} \frac{\partial}{\partial x}(v^2 - u^2) - \frac{\partial}{\partial y}(uv), \quad (2.2)$$

so that with cyclic boundary conditions,

$$\overline{v'\zeta'} = -\frac{\partial \overline{u'v'}}{\partial y}, \quad (2.3)$$

where the overbar denotes a zonal average and  $\bar{v} = 0$ . [Equation (2.3) also holds, locally in  $x$  if the average is a time or ensemble average provided that the eddy statistics are zonally uniform.] Averaging (2.1) thus gives

$$\frac{\partial \bar{u}}{\partial t} = \overline{v' \zeta'} + \bar{F}_u - \bar{D}_u, \quad (2.4)$$

where, again,  $\bar{v} = 0$ , and this result again also holds in a time or ensemble average if the eddy statistics are zonally uniform.

Typically, there will be little direct forcing of the mean momentum, and if friction is parameterized by a linear drag, then

$$\frac{\partial \bar{u}}{\partial t} = \overline{v' \zeta'} - r\bar{u}, \quad (2.5)$$

where  $r$  is an inverse frictional time scale. Now consider the maintenance of this vorticity flux. The barotropic vorticity equation is

$$\frac{\partial \zeta}{\partial t} + \mathbf{u} \cdot \nabla \zeta + v\beta = F_\zeta - D_\zeta, \quad (2.6)$$

where  $F_\zeta$  parameterizes the stirring of barotropic vorticity and  $D_\zeta$  represents dissipation. Linearize about a mean zonal flow to give

$$\frac{\partial \zeta'}{\partial t} + \bar{u} \frac{\partial \zeta'}{\partial x} + \gamma v = F'_\zeta - D'_\zeta, \quad (2.7)$$

where  $\gamma = \beta - \partial^2 \bar{u} / \partial y^2$  is the meridional gradient of absolute vorticity. From (2.7), form the pseudomomentum equation by multiplying by  $-\zeta' / \gamma$  and zonally averaging, whence

$$\frac{\partial M}{\partial t} - \overline{v' \zeta'} = -\frac{1}{\gamma} (\overline{\zeta' F'_\zeta} - \overline{\zeta' D'_\zeta}), \quad (2.8)$$

where  $M = -\overline{\zeta'^2} / 2\gamma$  is the pseudomomentum. From (2.5) and (2.8) we obtain

$$\frac{\partial \bar{u}}{\partial t} - \frac{\partial M}{\partial t} = -r\bar{u} + \frac{1}{\gamma} (\overline{\zeta' F'_\zeta} - \overline{\zeta' D'_\zeta}), \quad (2.9)$$

and in a statistically steady state,

$$r\bar{u} = \frac{1}{\gamma} (\overline{\zeta' F'_\zeta} - \overline{\zeta' D'_\zeta}). \quad (2.10)$$

The terms on the right-hand side represent the stirring and dissipation of pseudomomentum, and in steady state their sum must integrate to zero. In a meridionally localized stirring region the first term can be expected to be positive; thus, meridionally localized but otherwise relatively unstructured vorticity stirring will give rise (for  $\gamma > 0$ ) to an eastward mean zonal flow in the region of the stirring, with a westward flow north and south of the stirring region. These equations represent the well-known physical argument that stirring gives rise to Rossby wave generation, and that momentum will converge in the region of stirring as the Rossby waves propagate away and dissipate.

If the stirred region is sufficiently broad, then multiple jets may form within the stirring region (e.g., Vallis and Maltrud 1993; Lee 1997). In that case, the mechanism

of jet formation is often expressed in terms of an inverse energy cascade to larger scales, inhibited by the formation of Rossby waves, leading to the preferential formation of zonal flow. However, such jets may still be thought of as being maintained by the stirring of pseudomomentum, but the pseudomomentum stirring and dissipation are organized by the jet structure itself even though the vorticity stirring  $F_\zeta$  may be homogeneous. In the earth's atmosphere, the stirring region (i.e., the midlatitude baroclinic zone) is relatively narrow in the sense that there is normally only one region of eddy driven eastward flow in the mean; however, the baroclinic zone is typically wider than the instantaneous jet itself, and the jet may thus meander within the baroclinic zone.

### b. Source of stirring in a baroclinic atmosphere

The stirring that might generate such jets arises from baroclinic instability or, more precisely, from the transfer of energy from baroclinic to barotropic modes. To see this, consider the two-layer quasigeostrophic equations

$$\frac{\partial q_i}{\partial t} + J(\psi_i, q_i) = 0, \quad i = 1, 2, \quad (2.11)$$

where

$$q_i = \nabla^2 \psi_i + F(\psi_j - \psi_i) + \beta y, \quad j = 3 - i, \quad (2.12)$$

and  $F$  is the inverse square deformation radius. If this is decomposed into barotropic and baroclinic modes in the standard way, the evolution equation for the barotropic mode becomes

$$\frac{\partial}{\partial t} \nabla^2 \psi + J(\psi, \nabla^2 \psi + \beta y) = -J(\tau, \nabla^2 \tau), \quad (2.13)$$

where  $\psi = (\psi_1 + \psi_2) / 2$  and  $\tau = (\psi_1 - \psi_2) / 2$ . The term on the right-hand side is just the forcing of the barotropic mode by the baroclinic mode and, although not sign definite, it generally leads to a transfer of energy into the barotropic mode as part of the baroclinic life cycle. Such stirring by baroclinic eddies thus gives rise to momentum convergence and is the ultimate cause of the surface westerly winds in midlatitudes. The vorticity flux producing the zonal jet will, of course, fluctuate simply because baroclinic activity fluctuates, partly in response to variations in the zonal shear itself and partly because it is a turbulent, chaotic system, and these fluctuations will give rise to variations in the zonal index (e.g., Feldstein and Lee 1998; Lorenz and Hartmann 2001). Although such variations will be largely barotropic, the stirring will be dependent in part on the barotropic flow, because the evolution equation of  $\tau$  involves  $\psi$ , and this may lead to feedbacks between the jets and the stirring. For example, the presence of surface drag may generate a shear from the barotropic flow, and this in turn may produce baroclinic activity and

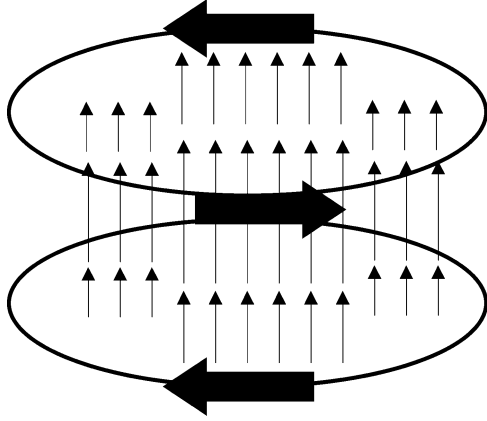


FIG. 1. Circulation pattern induced by anomalous vorticity fluxes. The light arrows represent time- or ensemble-mean fluxes of eddy vorticity. The contours represent circuits for the calculation of circulation. The heavy arrows on the circuits represent the circulation that results from the eddy vorticity flux.

enhanced stirring (Robinson 2000). In our numerical simulations, we will restrict ourselves to the simpler barotropic case and will model the stirring simply by a random process with time and space scales chosen to roughly mimic those of baroclinic instability, with no direct dependence on the jet itself.

### c. Patterns of variability

Because the stirring is produced by a chaotic process it will fluctuate, and this will produce a response in the zonal wind field and the associated circulation. In particular, a fluctuation in the vorticity flux that has a simple meridional structure will produce a dipolar structure in the pressure or streamfunction field. To illustrate this, Fig. 1 shows an idealized localized northward eddy flux of vorticity (light arrows). Two circuits are shown as solid contours with circulation  $\Gamma = \oint u_t ds$ , where  $u_t$  is the velocity component tangential to the circuit. With the mechanical damping, we have

$$\frac{d\Gamma}{dt} = \oint u_n \zeta ds - r\Gamma, \quad (2.14)$$

where  $u_n$  is the velocity component normal to the (right-hand oriented) circuit. Because the flow is incompressible,  $\oint u_n ds = \oint (\partial\psi/\partial s) ds = 0$ , where  $\psi$  is the streamfunction. Thus, if an overbar (e.g.,  $\bar{u}$ ) denotes the average along the circuit, and a prime ( $u'$ ) the departure from this average, then

$$\frac{\partial \bar{u}_t}{\partial t} = \overline{u'_n \zeta'} - r\bar{u}_t, \quad (2.15)$$

and for the time average in addition to the circuit average

$$\bar{u}_t = \overline{u'_n \zeta'}/r. \quad (2.16)$$

Thus, a time-mean eddy flux of vorticity out of the

circuit will give rise to a mean circulation. In Fig. 1, to the north of the maximum vorticity flux, a cyclonic circulation will result, and to the south, an anticyclonic circulation. This change in sign of the circulation corresponds to a change in sign of the streamfunction; if the pattern of vorticity flux is interpreted as an anomaly from a climatology, the eddy vorticity flux then produces a dipolar circulation anomaly. If the fluctuation is zonally symmetric, then the circulation anomaly will extend around the hemisphere. If the fluctuation is confined to some region of longitude as in Fig. 1, then the fluctuation will be a zonally localized dipole, rather like the NAO.

The argument above provides information about the circulation around a closed loop and, formally, says nothing about the zonal velocity itself. [Of course the loop may extend around a latitude circle, in which case  $u_t$  is the zonal velocity and we recover (2.5).] However, we may also expect that locally stronger stirring will give rise to a locally stronger and more variable zonal jet. If the zonal scale over which the eddy statistics vary is longer than the meridional scale, then the first term on the right-hand side of (2.2) will be smaller than the second term, after time averaging, and (2.3) will *approximately* hold. Similarly, the zonal advection of momentum in (2.1) will be smaller than that of meridional momentum, and the upshot is that (2.5) will *approximately* hold, with the overbar representing an average over a zonal sector without the need for complete zonal averaging.

Thus, in regions where stirring is enhanced over a reasonably broad zonal extent—for example, the storm track regions—we expect to observe two related phenomena: 1) a stronger and more variable zonal jet; 2) streamfunction or pressure anomalies that have the dipolar structure noted above. Furthermore, because these are anomaly fields, any diagnostic that seeks to economically represent the patterns of pressure or streamfunction variability, for example the EOFs, will also have a dipolar structure, and this is of course the characteristic pattern of the NAO. The latitude of the node of the mean streamfunction dipole will be that at which the mean vorticity flux is largest, and this is latitude of the mean jet itself. However, the distribution of the anomalous fluxes need not coincide with that of the mean fluxes, and we will see in section 4 that the node of the EOF of the streamfunction, representing the variability of the pattern, is often poleward of the jet and associated with a change in the position of the jet.

### 3. Numerical model

To see whether eddy stirring can indeed produce the characteristic spatial patterns and temporal variability of annular modes and the NAO, we integrate the barotropic vorticity equation on the sphere; namely,

$$\frac{\partial \zeta}{\partial t} + J(\psi, \zeta + f) = S - r\zeta + \kappa \nabla^4 \zeta. \quad (3.1)$$

The notation is standard, with  $f = 2\Omega \sin\vartheta$ , where  $\vartheta$  is latitude,  $\zeta$  is vorticity, and  $\psi$  is streamfunction. The model is spectral with the nonlinear term evaluated without aliasing using a spectral transform method. Typically, the model is run at a resolution of T42 with test integrations at T84; this is more than adequate resolution because our concern is large-scale patterns. The last two terms on the right-hand side of (3.1) are a linear drag and a term to remove the enstrophy that cascades to small scales, these being the simplest parameterizations of those processes that remove momentum and enstrophy from the flow. The coefficient  $\kappa$  depends on the model resolution, for that term is a subgrid-scale closure. The linear drag has some physical grounding in Ekman layer theory, and for a barotropic representation of the atmosphere reasonable values of  $r$  are of order 1/5–1/10 days<sup>-1</sup>.

The term  $S$  represents stirring of the barotropic flow by baroclinic eddies, and we represent this by a Markov process, similar to that employed in Maltrud and Vallis (1991). Typically, we choose to excite a small range of wavenumbers,  $n_{\min} < n < n_{\max}$ , where  $n$  is the total wavenumber and  $n_{\min} = 10$  and  $n_{\max} = 14$ , except that small zonal wavenumbers, including the zonal flow, are excluded from the forcing. (Specifically we exclude modes with  $m = 0$  to  $m = 3$ .) Ideally, we might prefer to not impose any particular time scale on the variability of the model fields, but a white noise forcing (which has equal amplitudes at all time scales) is not particularly realistic or appropriate, because the highest realizable frequencies would be time step dependent and would not generate much response in the vorticity field, leading to a very noisy solution. Rather, we choose the random forcing to have a decorrelation time scale of about 2 days, similar to that of baroclinic instability. We satisfy this by making the forcing in each wavenumber  $S_{mn}$  to be itself the outcome of the stochastic process:

$$\frac{dS_{mn}}{dt} = \dot{W}_{mn} - \frac{S_{mn}}{\tau}, \quad (3.2)$$

where  $\dot{W}$  is a white noise process (a different realization for each wavenumber) and the parameter  $\tau$  determines the decorrelation time of the forcing. To implement (3.2), we use the related finite difference equation (see appendix):

$$S_{mn}^i = (1 - e^{-2dt/\tau})^{1/2} Q^i + e^{-dt/\tau} S_{mn}^{i-1}, \quad (3.3)$$

where  $Q^i$  is chosen randomly and uniformly  $\in (-A, A)$ , where  $A$  determines the overall forcing amplitude,  $dt$  is the model time step, the superscript  $i$  is the time step index, and  $\tau$  is the prescribed decorrelation time of the forcing, which we choose to be 2 days. This spectral forcing is then transformed to physical space, where it is masked such that it has a nonnegligible amplitude

TABLE 1. Parameters for the baseline numerical experiments. Experiments with varying parameters are branches off these with a single parameter varied, unless noted. The decorrelation time scale of the forcing is always 2 days. The stirring region has a Gaussian distribution in latitude,  $\exp[(\vartheta - \vartheta_0)^2/2\sigma_\vartheta^2]$ , and the “half-width” is actually the std dev  $\sigma_\vartheta$  of this. The zonally asymmetric forcing for A1 is described by (5.1), with  $B = 1$  and  $\sigma_x$  corresponding to 45°.

Experiment	Meridional half-width of stirring region	Damping time scale (days)	Zonally symmetric
Z1	12°	6	Yes
A1	12°	6	No

only in a midlatitude band, centered at 45° with about a 25° width. For some experiments it is also made statistically zonally nonuniform; that is, it is enhanced in a longitudinally confined region to mimic the effects of enhanced stirring in storm tracks. As for the symmetric case it is constructed to have zero projection on the zonally symmetric flow (modes with  $m = 0$ ) at all times.

Apart from this meridional masking and the choice of the scale of the stirring, the stochastic forcing is relatively unstructured, and the resulting momentum flux convergences result from the nonlinear dynamics of the model. This type of stochastic model differs from that used in, for example, Branstator (1992) or Whitaker and Sardeshmukh (1998), in which the model is linear and the mean flow is taken from observations or a GCM. Here, the model is nonlinear, and it is the stochastic forcing in conjunction with nonlinear dynamics that generates the mean flow, and that is important for its pattern of variability.

Given the general form described above, for a given set of parameters the model is first spun up, and the integration continued for a period of order 10 000 days over which diagnostics are obtained. The main parameters we have varied are 1) the strength of the forcing and its degree of zonal asymmetry, that is, the strength of the storm track; 2) the meridional width of the forcing region; and 3) the strength of the friction (the surface drag). Regarding parameter 1, the overall strength of the forcing is tuned to produce a zonal jet of reasonable strength. Note that the forcing is meant to produce an eddy momentum flux convergence that is responsible for producing nonzero *surface* winds in the midlatitude atmosphere. However, a barotropic model is often thought of as being representative *vertically integrated* flow. Such an ambiguity is unavoidable in a model with only one degree of freedom in the vertical; our control integration uses a forcing that produces a zonally averaged wind of about 10 m s<sup>-1</sup>. Regarding parameter 2, in our control integration, our forcing strength has a Gaussian distribution in latitude, centered at 45°, with a meridional half-width of 12°. This is varied from 3° to being as wide as the hemisphere. Regarding parameter 3, the results are not sensitive to the strength of the friction when this is in the range 1/5–1/10 days<sup>-1</sup>, and most of the simulations presented here use 1/6 days<sup>-1</sup>. See also Table 1.

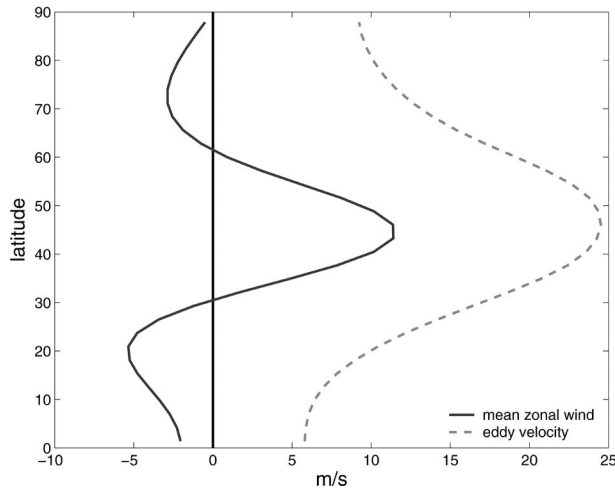


FIG. 2. The time- and zonally averaged zonal wind (solid line) from the zonally symmetric numerical model Z1 (see Table 1). The dashed line is the rms (i.e., eddy) velocity. The stochastic forcing is zonally uniform and is a Gaussian distribution in the meridional direction, centered at  $45^\circ$  with  $12^\circ$  half-width.

#### 4. Results with zonally symmetric forcing

##### a. Mean state for zonally symmetric model

A typical time and zonally averaged zonal wind, and the rms (i.e., eddy) velocity are illustrated in Fig. 2 for the pivot experiment Z1. A strong westward jet emerges in the region of the forcing, flanked by two eastward jets, rather stronger on the equatorial side. Consistently, the mean position of the jet is somewhat poleward of the center of the stirring, and this polewards offset increases slightly as the forcing strength increases. The eddy velocities are of the same order of magnitude, albeit a little larger than, the zonally averaged velocity, a characteristic also of the flow in the earth's atmosphere. The pseudomomentum stirring and dissipation responsible for the mean jet are illustrated in Fig. 3. The pseudomomentum forcing is large and positive in the jet center, with a fairly narrow distribution. The distribution of the pseudomomentum dissipation is broader, reflecting the meridional propagation of Rossby waves away from the stirring region.

The natural meridional scale of a jet in homogeneous barotropic turbulence is determined by the eddy kinetic energy, and the value of  $\beta$  and friction (e.g., Maltrud and Vallis 1991; Smith et al. 2002). As noted above, if the meridional extent of the forcing region is allowed to become larger than that jet scale, alternating jets may form within the forcing region. This phenomena is illustrated in Fig. 4 when the forcing has no meridional localization, although the forcing and resulting eddies are too strong for multiple jets to be produced.

##### b. Variability

Now consider the variability of a single, eddy driven zonal jet. Consider the momentum equation (2.5) and

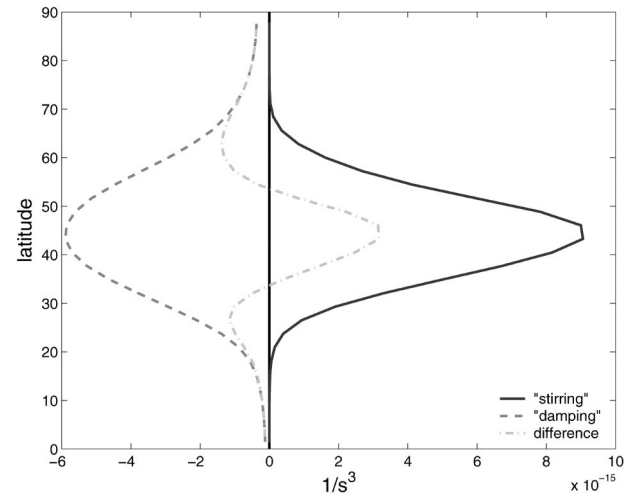


FIG. 3. The pseudomomentum stirring  $\overline{F_\xi^{\prime\prime}}$  and dissipation  $\overline{D_\xi^{\prime\prime}}$  and their sum [see Eq. (2.10)] for Z1. The distribution of dissipation is broader than the forcing, resulting in an eastward jet where the stirring is centered, with westward flow on the flanks.

suppose that the vorticity flux is such as to produce an eastward jet in midlatitudes, and that its magnitude fluctuates temporally but that its meridional structure remains fixed. Then the zonally averaged zonal wind will fluctuate in place—it will pulse—and the associated EOF of the zonal wind will be similar to that of the mean wind (Fig. 5a). Since at each instant the pressure field (the streamfunction) and the velocity are linearly related, the associated variability in the pressure field can be expected to be a dipole. If the zonal wind fluctuates in this way, the node of the pressure EOF will coincide with the maximum of the jet, which in turn occurs where the stirring is strongest. The other dominant mode of variability might be termed a wobbling of the zonal jet, that is, an oscillation in its latitude without necessarily any change in amplitude (Fig. 5b).

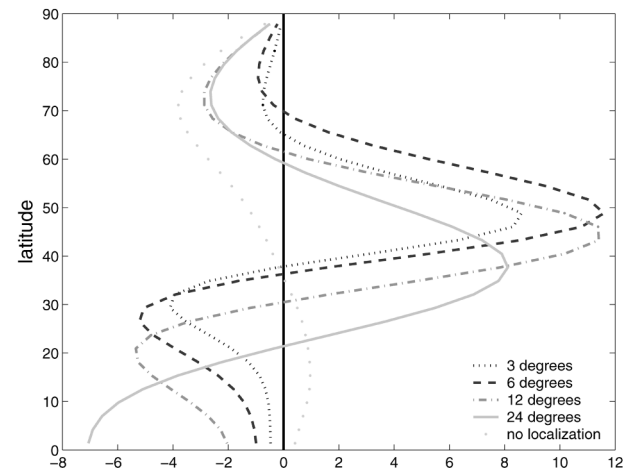


FIG. 4. Time- and zonally averaged zonal flow in experiments with varying half-widths of the forcing zone. If the forcing zone is narrow, then a single eastward jet forms in the region of the forcing.

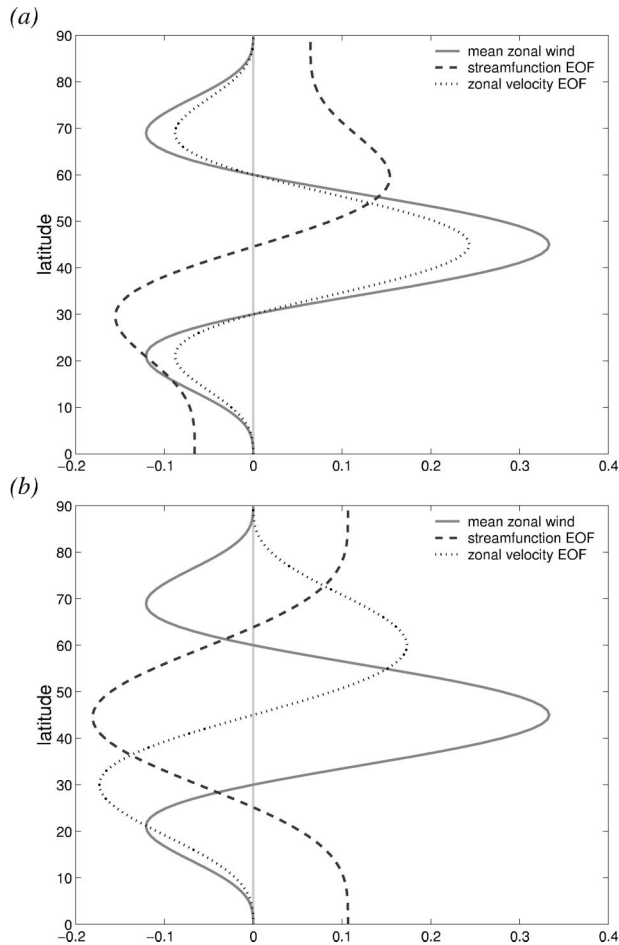


FIG. 5. (a) Schematic of the leading EOFs associated with a pulsing jet. The solid line is the mean zonal wind itself, the dotted line is the EOF of the zonal velocity, and the dashed line the EOF of the pressure or streamfunction field. (b) As in (a), but for the leading EOF associated with a wobbling or oscillating jet.

Both pulsing and wobbling behavior frequently occur in numerical simulations, and one factor determining which is dominant is the width of the stirring region. If the stirring region is narrow (narrower than the resulting jet), then the jet position is effectively fixed and the first EOF resembles the jet itself. If the stirring region is wider than the natural width of a single jet, but not sufficiently wide to support two jets, the jet's position can vary within the stirred region. The behavior in these two cases is illustrated in Fig. 6. (One-dimensional EOFs are constructed from daily fields; two-dimensional EOFs are constructed from the fields after applying a 10-day running average.)

With a stirred region of similar meridional extent to that of the baroclinic zone on earth a wobbling or a "mixed" mode tends to prevail (Fig. 7), with the second EOF looking more like a pulse. The first EOF of the streamfunction is dipolar, with a node somewhat poleward of the mean position of the jet and the lower band more or less coincident with the mean position of the

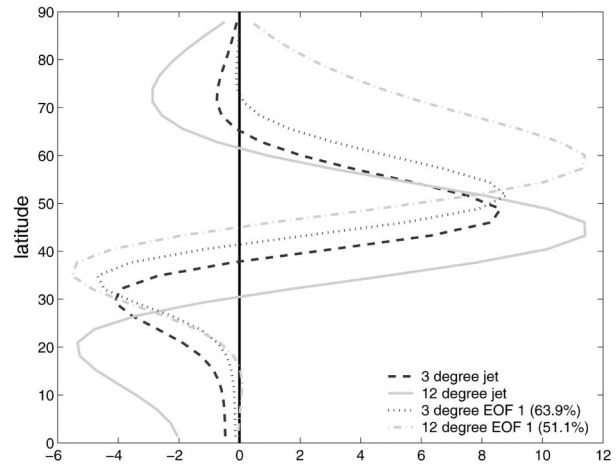


FIG. 6. The mean value and the first EOF of the zonally averaged zonal wind simulations with a narrow stirring region (approximately  $3^\circ$  half-width) and a broader stirring region (approximately  $12^\circ$  half-width). For the narrow forcing region, the first EOF is a almost a "pulse," with a structure similar to that of the jet itself. For a wider forcing region, the first EOF is closer to a "wobble." Figures in parentheses indicate variance accounted for.

jet. These structures are apparent in both the EOF of the zonally averaged fields, and in the zonally averaged EOF of the two-dimensional fields (not shown). The first EOFs are typically well separated from the other EOFs. Similar structures are seen in the observations (Feldstein and Lee 1998; Lorenz and Hartmann 2001) and in simulations with a general circulation model (Cash et al. 2002). Indeed Feldstein and Lee (1998) characterize the EOFs of the Northern and Southern Hemispheres as being either a strengthening and weakening of the jet or a latitudinal movement of the jet, although the interpretation is complicated by additional variations in the subtropical jet.

Although useful as descriptive phrases, the pulsing and wobbling modes are not necessarily distinct physical modes. Recall that the mean wind is somewhat poleward of the center of the stirring, because of predominantly equatorward breaking of the Rossby waves. If the stirring is stronger, the jet is not only stronger but is pushed slightly poleward, and the pulse and the wobble are synchronized. The EOFs are describing this in the most economical way possible, subject to their orthogonality.

### c. Two-dimensional patterns

When one looks at the EOF of the two-dimensional fields, the zonal average of the first EOF (of either velocity or streamfunction) is usually very similar to the EOF of the zonally average field, although the subsequent EOFs are less distinct. The first EOF normally is well separated from the others, although the variance accounted for is typically less than 20%. The first EOF of the two-dimensional streamfunction is illustrated in

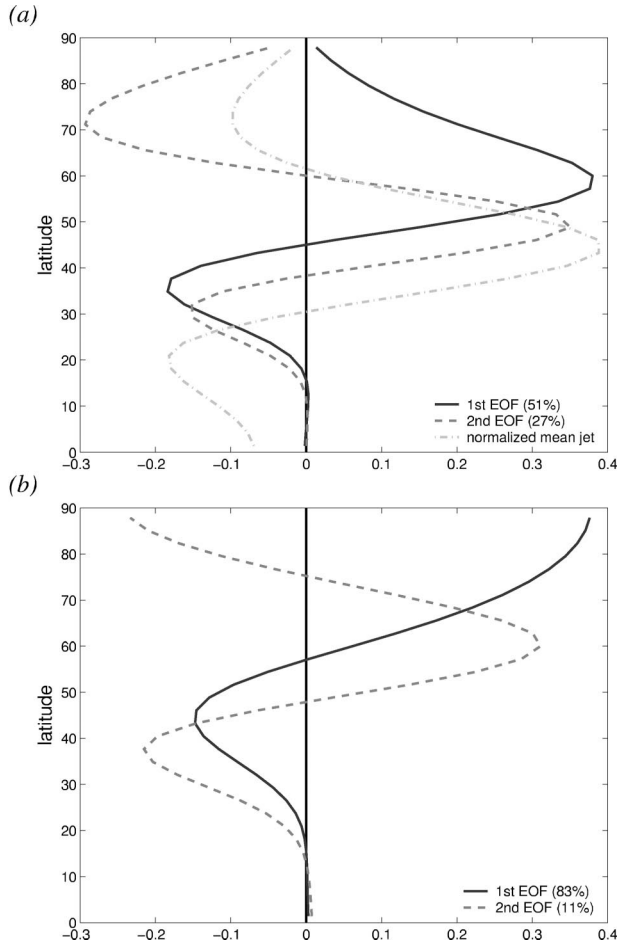


FIG. 7. (a) The first two EOFs (solid and dashed, respectively) of the zonally averaged zonal wind forced in the zonally symmetric configuration Z1. The solid line corresponds to a wobbling zonal wind, the dashed to a pulsing zonal wind. The light dotted line is the mean zonal wind. (b) Corresponding EOFs of the zonally averaged streamfunction.

Fig. 8. It is nearly zonally symmetric and may be taken as a definition of the annular mode of this model. Now, even though the time-averaged flow is zonally symmetric, the leading EOF itself is not guaranteed to be zonally symmetric. (Suppose, for example, that all the model variability occurred at zonal wavenumber 5, then the first two EOFs would show wavenumber-5 patterns, in quadrature with each other.)

Nevertheless, the presence of a zonally symmetric first EOF should not lead one to conclude that there is a necessarily strong mode of hemispheric-wide variability in the model. The EOF analysis is merely seeking the most economical description of model variability. In particular, in most of the integrations we have examined the zonal flow does not vary synchronously across the hemisphere. The one-point correlation function shows this quantitatively (Fig. 9). In the meridional direction, the dipolar structure of the EOF can be seen in the correlation function, especially the one centered

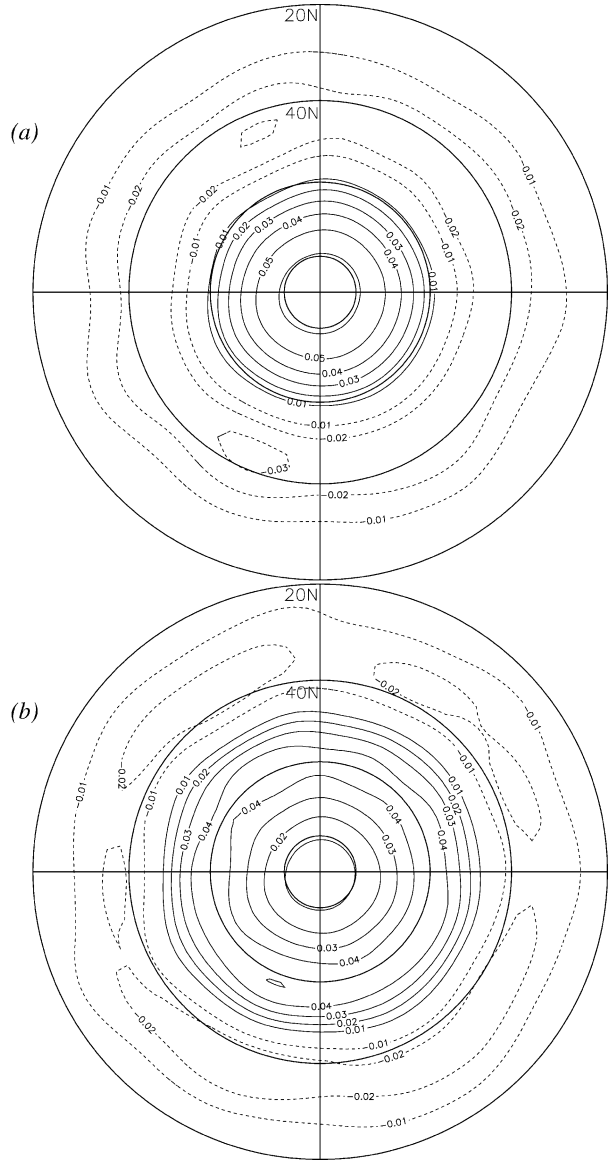


FIG. 8. (a) The leading EOF of the streamfunction (with a 10-day running average) when the model is forced in the zonally symmetric configuration Z1. The first and second EOFs account for 15% and 5% of the variance, respectively. (b) Leading EOF of the (10 day averaged) zonal wind. The first two EOFs account for 11% and 5% of the variance. The zero contours are omitted.

at the pole. The zonal scale of the correlation is related to the scale of the energy containing eddies, as one might expect given that the spatial correlation function is essentially the Fourier transform of the variance of that variable (so the velocity correlation function is the Fourier transform of the energy spectrum). Thus, large-scale hemispheric-wide correlations are associated with variance in the  $m = 0$  mode and, even though zonal jets are naturally produced by eddies on the sphere or  $\beta$  plane, the covariability of flow around a circle of latitude may be relatively weak. Ultimately, the importance or

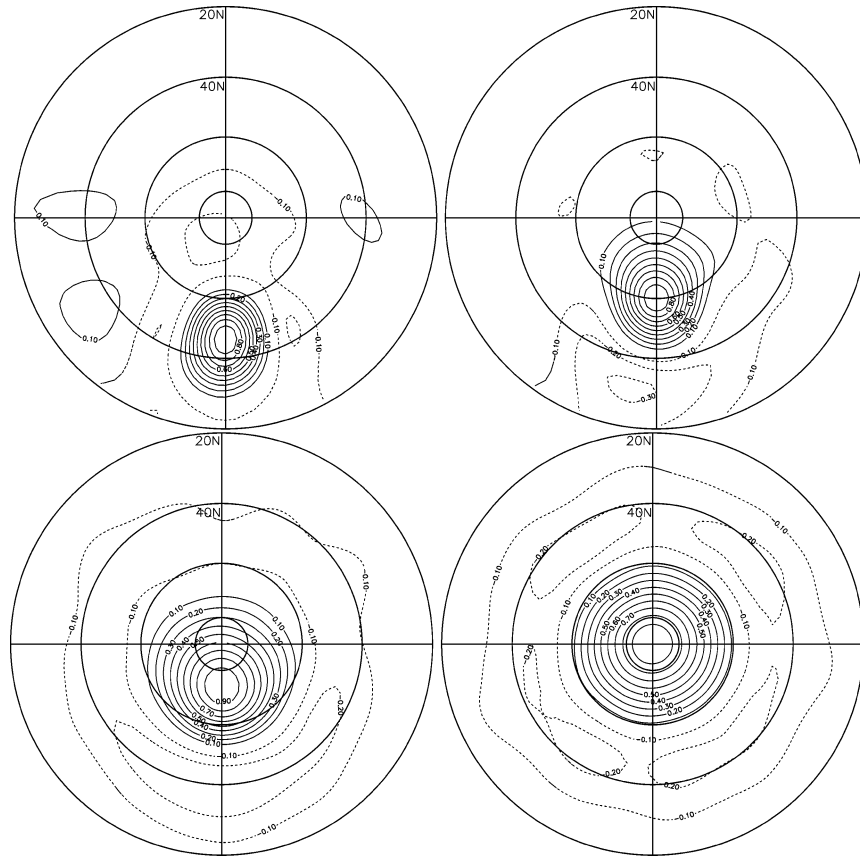


FIG. 9. The one-point autocorrelation of the streamfunction for the same integration as Fig. 8, for four different base points (which can be identified as the points where the correlation is one). Because the statistics are zonally symmetric, the longitude of the base points is unimportant. The zero contours are omitted.

meaningfulness of an annular mode is related to how much eddy energy is in the zonal modes, and this is a quantitative issue that can ultimately be settled only by an appeal to observations (see also Cohen and Saito 2002). The spatial structure of these correlations are in fact very similar to those found in various simulations with a general circulation model (Cash et al. 2002). There too the first EOF is almost zonally symmetric and meridionally dipolar, but there is little hemispheric-wide correlation.

We can obtain another sense of the hemispheric versus local nature of the variability by constructing the EOFs from a quadrant (i.e., regions  $90^\circ$  wide) rather than the full hemisphere. In both cases the flows are weighted to correct for the decrease in area with latitude before computing the EOFs, and these are illustrated in Fig. 10. The first EOF of the regional field is quite similar with that constructed from the full hemispheric field, consistent with the notion that it is the same mechanism producing the variations in the zonal velocity on a hemispheric and on a regional scale. (In fact, if the EOF computed from the zonally averaged flow is regressed onto the sector-averaged flow, the correlation of this

time series with the time series of the principal component in the sector is almost always over 95%.)

However, the variations in the various quadrants are not always in concert. To quantify this, we compute the correlations between the daily time series of the principal components (PCs) corresponding to the regional and hemispheric EOFs, and between two opposing quadrants. The values of these are

$$C(Z, Q1) = 0.61, \quad (4.1a)$$

$$C(Z, Q2) = 0.63, \quad (4.1b)$$

$$C(Q1, Q2) = 0.06. \quad (4.1c)$$

Here,  $C(Z, Q1)$  is the temporal correlation between the PCs of the first EOF from the zonally averaged flow and that of flow in a quadrant [and similarly for  $C(Z, Q2)$ ], and  $C(Q1, Q2)$  is the correlation between the flow in the two quadrants. The difference between  $C(Z, Q1)$  and  $C(Z, Q2)$  is solely due to the finite length of the time series, and so is a measure of the error due to that.

If there were a pure annular mode in the sense that the zonal velocity varied in unison on a hemispheric

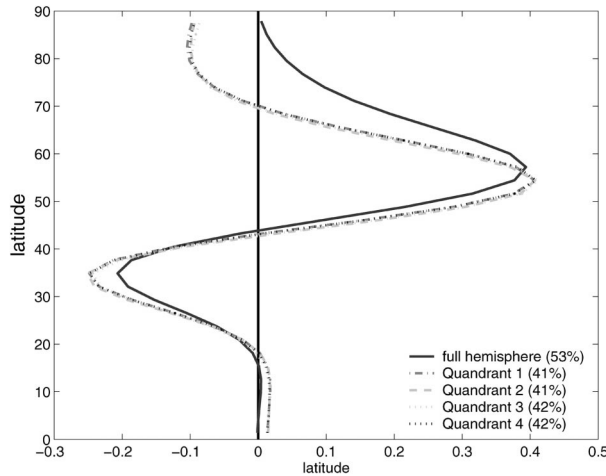


FIG. 10. The EOF calculated from the zonally averaged flow in the entire hemisphere and from the zonally averaged flow in four quadrants (various dashed lines, on top of each other) for Z1. If the hemispheric EOF is regressed onto data in any one quadrant, then its time series has a correlation of approximately 0.97 with that of the principal component in the quadrant.

scale, the correlations would all be unity. If the quadrants were completely independent, we would have

$$C(Z, Q1) = 0.5, \quad (4.2a)$$

$$C(Z, Q2) = 0.5, \quad (4.2b)$$

$$C(Q1, Q2) = 0. \quad (4.2c)$$

Clearly the flow here is something in between these extremes. One may conclude that, although similar dynamics are acting on both the regional and hemispheric scales (because the meridional structure of the respective EOFs are so similar), these dynamics do not necessarily act in unison. We cannot expect the real atmosphere to have quantitatively the same values as (4.1), but the qualitative picture is likely to be similar.

#### d. Low and high index states

As noted, the mean position of the jet is slightly poleward of the center of the stirring. The stronger the jet, the more poleward the mean jet position, as indicated in Fig. 11, although the effect is rather weak and the displacement of the jet is no more than  $5^\circ$ . However, a stronger jet is also noticeably narrower than a weak one, and the easterlies on its equatorial flank are noticeably stronger and extend farther poleward. In a model with a baroclinic subtropical jet, or the real atmosphere, the effect of this would be to enhance the separation between the eddy driven jet and the subtropical jet, and to make the midlatitude surface westerlies both stronger and slightly more poleward. Both of these effects are seen in the observations during high index states (Am-  
baum et al. 2001).

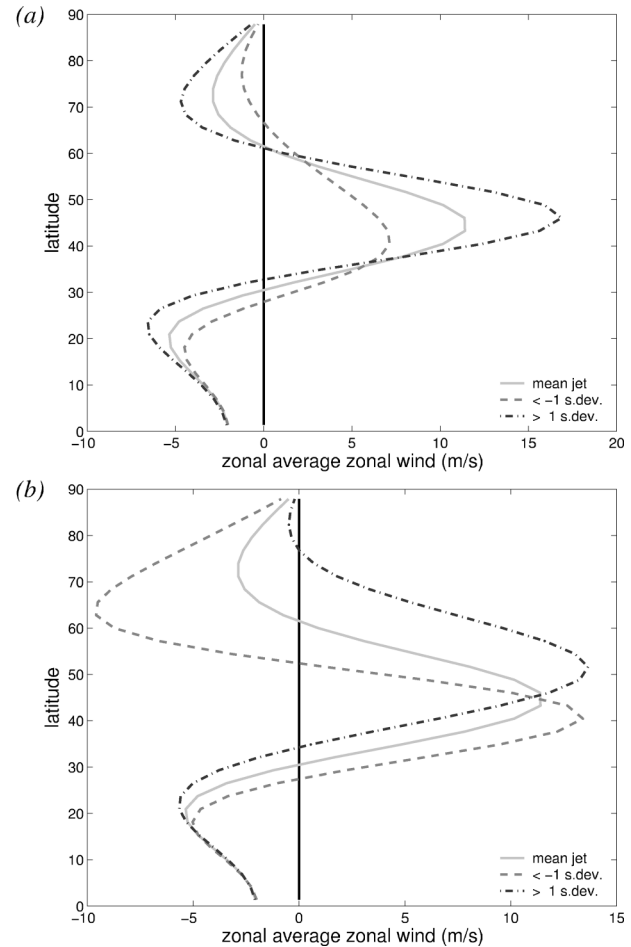


FIG. 11. (a) Composites of the zonally averaged zonal wind, averaged over periods when it is particularly strong or particularly weak, for experiment Z1. The mean jet is solid, the other lines corresponding to averages over periods when its peak value deviates by more than an std dev from the mean, as indicated in the legend. (b) Composite of the zonally averaged zonal wind, as in (a), except now the composites are averaged over periods when its first principal component exceeds or is less than an std dev from its mean.

## 5. Results from the zonally asymmetric model

Suppose we now enhance the stirring in a longitudinal region in order to roughly mimic the effects of a storm track. However, we keep the simple meridional structure used in the zonally symmetric case, and the stirring maximum is at the same latitude for all longitudes. Specifically, the longitudinal structure of the amplitude of the stirring is

$$|F_z| = A\{1 + B \exp[-(x - x_0)^2/2\sigma_x^2]\}, \quad (5.1)$$

where  $A$  and  $B$  are constants;  $A$  determines the strength of the uniform background stirring and  $B$  that of the zonal inhomogeneity, centered around longitude  $x_0$ . We have conducted experiments with  $B$  ranging from 0 to about 10, with a value of order unity best representing the enhanced stirring of the storm track regions over the

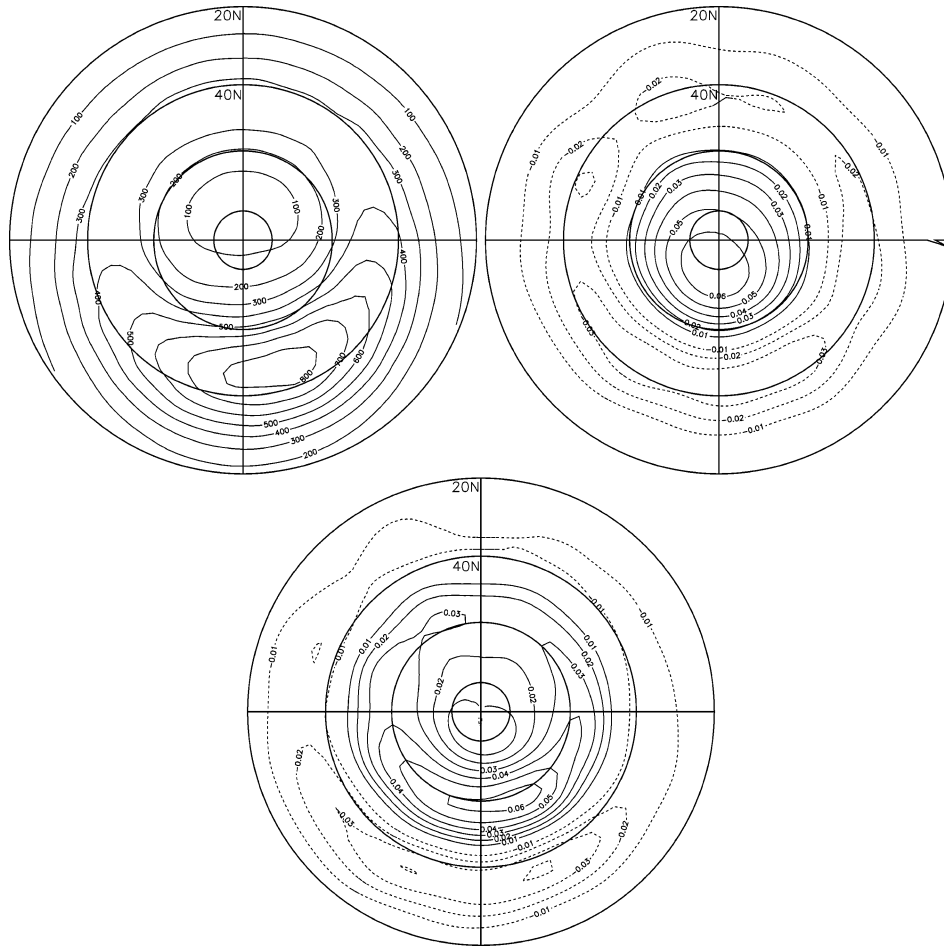


FIG. 12. (left) Eddy kinetic energy when the model is forced in a zonally asymmetric configuration with a single enhanced region of forcing (A.1). (right) The leading EOF of the streamfunction (18% variance accounted for; 6% variance in the second EOF). (bottom) The leading EOF of the zonal wind (12% variance; 6% variance in the second EOF). The zero contours are omitted.

Atlantic and Pacific. The parameter  $\sigma_x$  determines the zonal width of the enhanced stirring region.

Figure 12 shows the fields of eddy kinetic energy and the first EOF in an asymmetric integration (A.1) with  $B = 1$  and  $\sigma_x = 45^\circ$ , producing an eddy-rich region roughly comparable to the major ocean storm tracks. The meridional half-width of the forcing is  $12^\circ$ . The eddy kinetic energy is a direct reflection of the enhanced stirring and, clearly, the EOF is centered around the enhanced stirring and reflects the more vigorous activity in that region. The localized dipole structure of the streamfunction is similar to that appearing in zonally asymmetric GCMs (e.g., CKV) and in the observations (e.g., Ambaum et al. 2001). This structure is fairly robust to variations in parameters. For example, Fig. 13 shows the EOF is a similar zonally asymmetric configuration, but when the forcing region has only a  $6^\circ$  half-width, a qualitatively similar structure is seen.

The one-point correlation function (Fig. 14), with a

base point at the longitude where the EOF is a maximum, picks up the meridional dipole structure of the EOF, just as in the zonally symmetric case. In the zonal direction, the correlation function is somewhat more localized than the EOF and is not, in fact, very dissimilar from that in the zonally symmetric case (Fig. 9). The day-to-day synoptic activity in the two cases is rather similar, but in the zonally asymmetric case there is a slight preference for dipole structures to form in the region of enhanced stirring, and this is detected by the EOF analysis. In the zonally symmetric case, similar two-dimensional structures form locally, but with no longitudinal preference and, as a consequence, the first EOF is almost zonally uniform.

We also calculated the EOFs based solely on the fields in the region on the enhanced stirring, as well as the EOFs in the opposite quadrant. The EOFs in the enhanced stirring region show a similar dipole structure to those of Fig. 12 and, in an analogous fashion to (4.1), we calculate

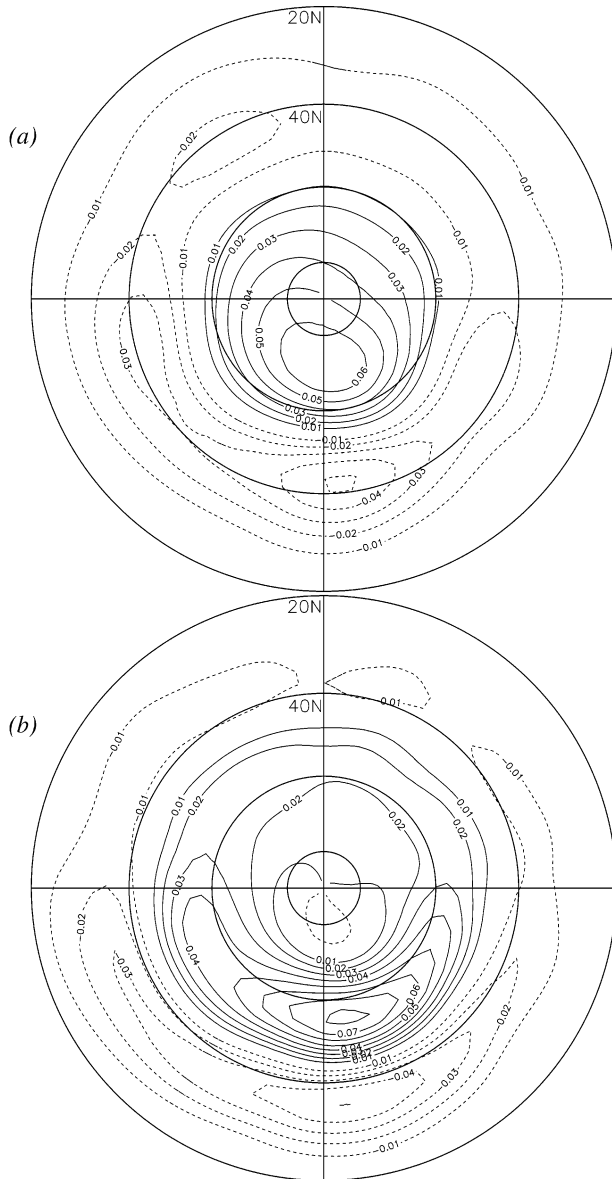


FIG. 13. (a) The leading EOF of the streamfunction (15% variance accounted for; 7% variance in the second EOF). (b) The leading EOF of the zonal wind (11% variance; 5% variance in the second EOF). These differ from the results in Fig. 12 only in that the forcing half-width is  $6^\circ$ .

$$C(Z, Q1) = 0.57, \quad (5.2a)$$

$$C(Z, Q2) = 0.72, \quad (5.2b)$$

$$C(Q1, Q2) = 0.11, \quad (5.2c)$$

where  $Q2$  denotes the region of enhanced stirring,  $Q1$  the opposite quadrant,  $C(Z, Q1)$  and  $C(Z, Q2)$  are the correlations between the principal components of the zonal EOF and the regional EOFs, and  $C(Q1, Q2)$  is the correlation between time series of the two regional EOFs. Thus, the principal component of the EOF constructed from the hemispheric flow correlates well with

the principal component of the EOF constructed in the region of enhanced stirring.

The structural similarity between the EOF and the teleconnection, and the similarity between the barotropic model, the GCM results of Cash et al. (2002), and the observations, are all suggestive of the robustness of the mechanism identified. We make two additional points. First, this is a nonlinear effect. If localized stirring is added to the linear barotropic vorticity equation, then the response is a superposition of beta plumes that trail westward from the source but which produce no vorticity flux, an effect familiar to most physical oceanographers. (Of course, one might construct a linear model to mimic the nonlinear effects, but one would have to specify the structure of the vorticity fluxes.) Second, the dipole structure that is evocative of the NAO arises robustly when the stirring is somewhat stronger than the zonal mean stirring [i.e., when  $B$  in (5.1) is of order one]. However, if the localized stirring is extremely intense (e.g.,  $B = 10$ ), then more exotic patterns (not shown) occur. Now the theory of section 2a becomes invalid because of the extreme zonal inhomogeneity.

## 6. Temporal structure

Apart from the signals due to El Niño and the seasonal cycle, the large-scale patterns of extratropical variability in the atmosphere appear to have a fairly red spectrum, with no really significant peaks (Feldstein 2000). However, it is unclear whether the power in these patterns continues to increase for time scales longer than the interannual—that is, whether the spectrum continues to redden for increasingly long time scales or whether it flattens out and whitens (see Stephenson et al. 2000). Notwithstanding that uncertainty, the decorrelation time scale associated with the NAO and similar patterns is of order 10 days. Now, in our numerical model the various possible time scales are the time scale of the forcing, a frictional time scale determined by the value of  $r$  in (3.1), a nonlinear eddy turnover time for some scale  $L$  given by  $L/|U_L|$ , where  $U_L$  is the velocity magnitude at the scale  $L$ , and a time scale associated with Rossby wave propagation  $\sim 1/(L\beta)$ . The external parameters are those associated with the forcing and friction—the eddy turnover time is ultimately given by the magnitude of the forcing and how effective it is in generating flow. If we choose our forcing decorrelation time to be of order a few days to represent baroclinic activity, then we must tune its magnitude to give flow velocities with a magnitude similar to those observed, and in that case the only remaining external free parameters are  $r$  and  $\beta$ .

Friction is one important element in determining the spectral response to the forcing, as we see from the linear version of (3.1). The equation is

$$\frac{\partial \zeta}{\partial t} + \beta \frac{\partial \psi}{\partial x} = S - r\zeta, \quad (6.1)$$

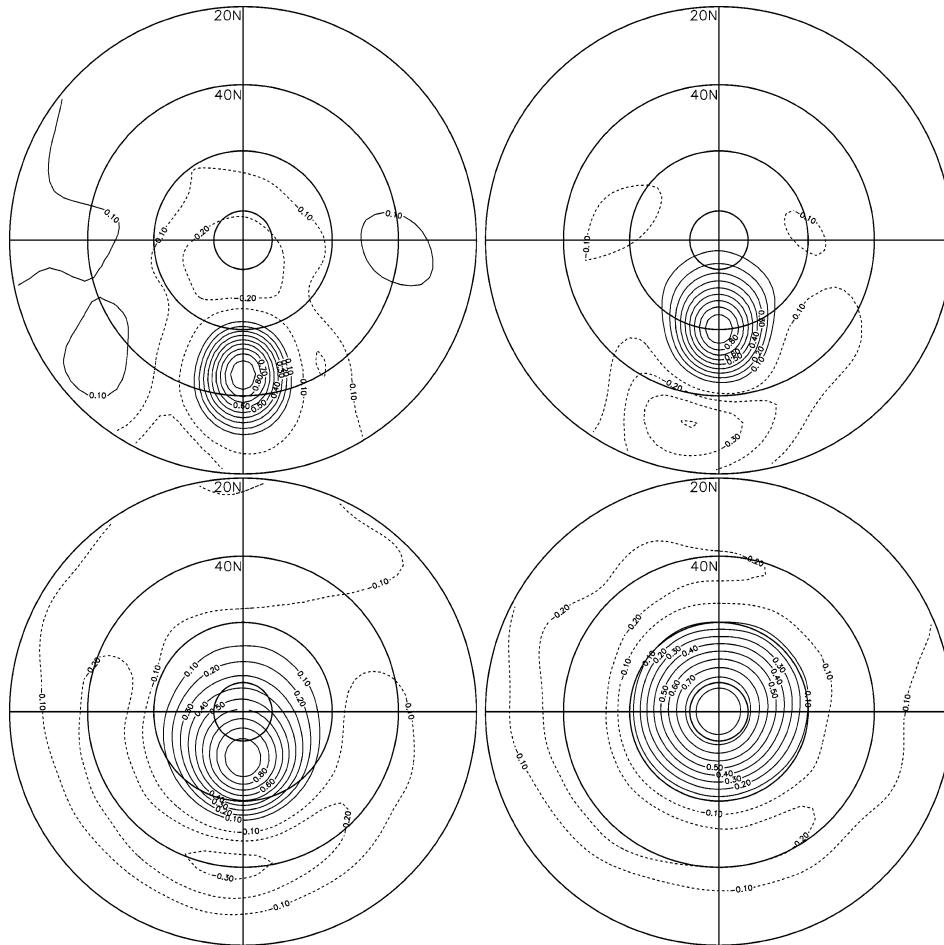


FIG. 14. The one-point correlation of the streamfunction, for the same zonally asymmetric integration as Fig. 12. The longitude of the base points is chosen to be along that of the strongest stirring, which is close to the longitude where the EOF has its maximum value. The zero contours are omitted.

and this can be solved analytically if the power spectrum of  $S$  is known. Assuming a solution of the form

$$\psi = \text{Re}\Psi e^{i(\mathbf{k} \cdot \mathbf{x} - \omega t)}, \quad (6.2)$$

where  $\text{Re}$  indicates the real part should be taken, and substituting into (6.1) gives

$$|\Psi|^2 = \frac{S_\omega^2}{[(k^2 \omega + \beta k_x)^2 + r^2 k^4]}, \quad (6.3)$$

and so the solution has a redder spectrum than the forcing. The solution is completed by the addition of the homogeneous problem, a decaying Rossby wave.

Numerical solutions of the nonlinear problem show that this effect contributes to, but is not, the whole story. In Fig. 15 we see a representative time series of the first EOF in a zonally symmetric simulation. [The EOF itself is first obtained using temporally low-passed (10-day running mean) data, but the figure shows the daily, unfiltered, values of the corresponding principal component.] Figure 16 shows the corresponding power spectra, which are characteristically red. The autocorrelation of

the first two EOFs is shown in Fig. 17, and these are of order 5–10 days. The wobbling mode typically has a longer decorrelation than the pulse, but these two modes are not wholly independent, and as the jet wobbles from one extreme latitude to another it passes through its mean location twice. For shorter frictional time scales the decorrelation time scale (the  $e$ -folding time scale) is similar to the frictional time scale, as expected in an Ornstein–Uhlenbeck-type process. However, inspection of Figs. 16a and 17b indicates that the correlation time scale does not increase as quickly as the frictional time scale increases; for frictional time scales of 6, 12, and 23 days, we find  $e$ -folding decorrelation time scales of 3.8, 4.4, and 7 days, respectively. Evidently, the chaotic dynamics of the large-scale fields are limiting the temporal correlations. The autocorrelation of the simulation with the higher damping (12 days) has virtually as much power at very long times as the simulation with a 23-day damping time scale, another indication that frictional effects are not the sole determinant of the power at low frequencies. Note that

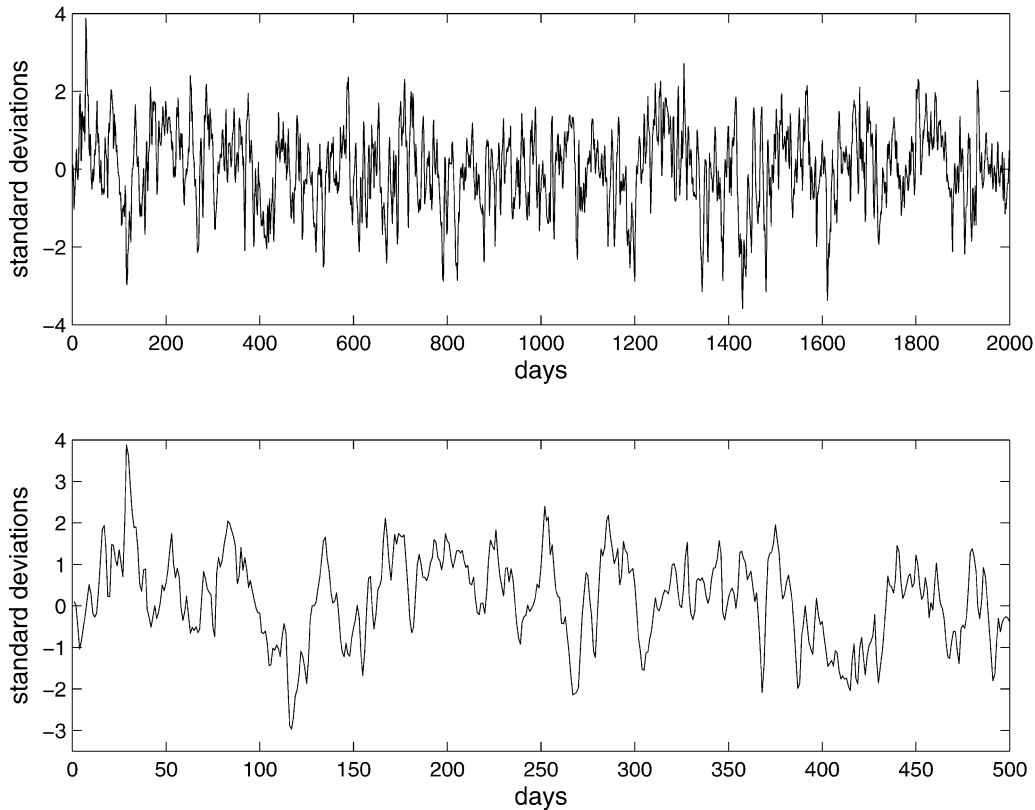


FIG. 15. Sample time series of the principal component of the leading EOF of zonal wind in the zonally symmetric integration Z1. (bottom) A blowup of the first 500 days of the top.

it is also apparent from the time series that quite long excursions from the mean are possible. For example, there are frequent excursions of order 100 days. [Long-term variability was also found by James and James (1992) in a simplified general circulation model, although the variability they found involved the subtropical jet, which is absent in this model.]

## 7. Summary and conclusions

We have presented a simple dynamical model of the North Atlantic Oscillation and the related annular modes. We have shown that spatial structures qualitatively similar to those associated with the North Atlantic Oscillation and annular modes can be robustly and easily reproduced with a stochastically forced, but nonlinear, nondivergent barotropic model. The stochastic forcing has a very simple spatial structure and need not be extensively tuned for the patterns to appear.

The model suggests that the NAO and annular modes are, essentially, two sides of the same coin. The (single) phenomenon is associated with variations in the mid-latitude circulation caused by fluctuating stirring from baroclinic eddies. The fluctuating stirring produces both a variation in the intensity and position of the zonal jet, and a dipolar circulation anomaly. This in turn leads to

a dipolar structure in the streamfunction (i.e., the pressure field) variability, and so a dipolar EOF, much as is observed.

If the eddy statistics are zonally uniform, then the leading EOF of the zonal velocity and the streamfunction are also approximately zonally uniform. Wave-mean flow interaction has produced variability in the zonally averaged flow, and this may be interpreted or defined as an annular mode. However, the variability of an annular mode is (in this interpretation) not the hemispheric-wide synchronous variability or heaving of a polar vortex. Rather, it is associated with the projection onto the zonally averaged flow of eddy dynamics.

The North Atlantic Oscillation is to be differentiated from the annular mode primarily by its scale, not its mechanism. The presence of an Atlantic storm track provides stronger stirring, and if the longitudinal extent of the storm track is greater than that of a single eddy, the same dynamics that produce variations of the zonally averaged flow will still act, just more intensely, over that region. Thus, the jet variations will be stronger here than elsewhere, and any measure of that variability, such as the first EOF of pressure or streamfunction, will show a dipole centered near the eddy activity. Now, when the stirring is stronger—that is, when the storm track is stronger—the barotropic jet is strengthened and tight-

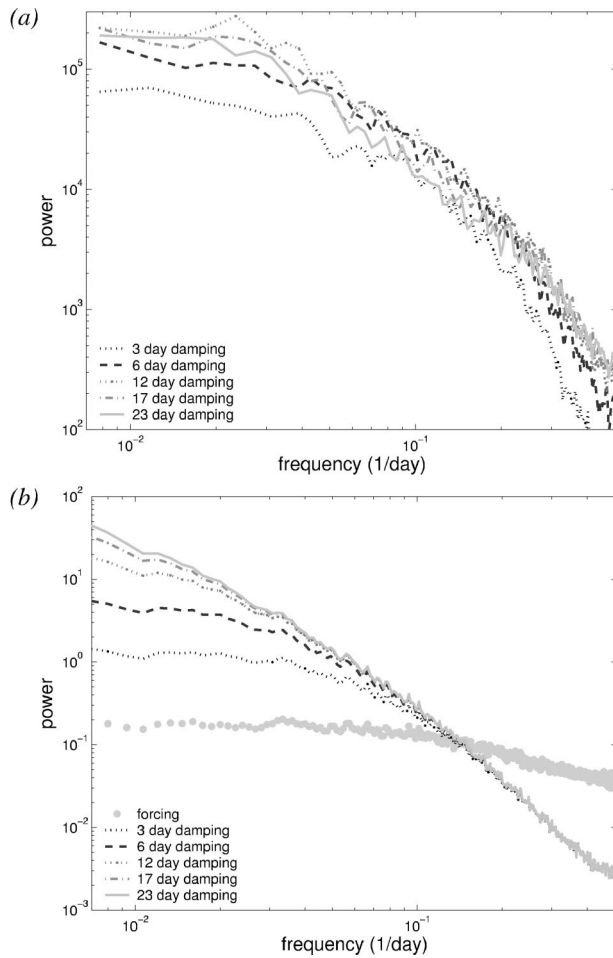


FIG. 16. (a) Power spectra of the principal components of the leading EOFs of the zonal wind in zonally symmetric integrations with varying values of the frictional parameter  $r$ , corresponding to frictional time scales of approximately 3, 6, 12, 18, and 23 days. (b) Power spectra of the stochastic process,  $dz/dt = S - rz$ , for the same values of  $r$  used in (a), and  $S$ , the stochastic forcing, also having the same power spectra as used to force the model.

ened, whereas any subtropical jet would be little altered. Thus, during periods of high eddy activity the eastward advection will be strongest at latitudes poleward of its mean position. Conversely, quiescent periods will have a weaker barotropic jet and the eastward advection will be somewhat equatorward of its mean position. Thus, at one extreme we can expect eddy-rich activity with a strong eastward jet somewhat poleward of its mean position; at the other extreme we expect weaker eddy activity with a weaker, slightly more equatorward jet. This is, of course, a characteristic of the NAO.

Another way of expressing this is to say that it is the organization of the baroclinic activity into spatially coherent large-scale patterns (i.e., storm tracks) that gives rise to coherent large-scale vorticity stirring, and this in turn produces patterns like the NAO. Because the mean amplitude of the vorticity stirring varies zonally, the eddy forcing has a stationary component (i.e., there is

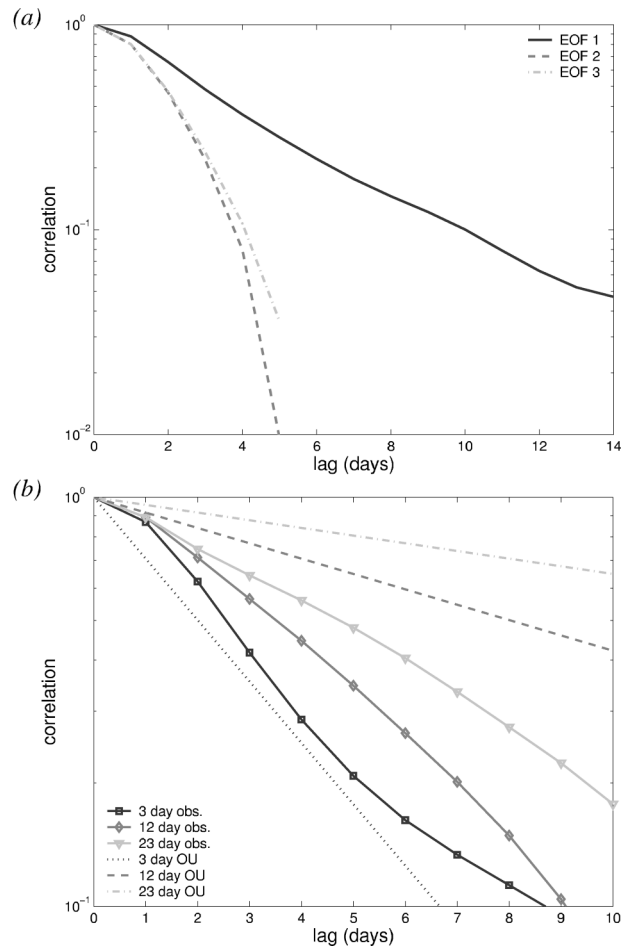


FIG. 17. (a) Autocorrelation of the PCs of the first two EOFs of the zonal wind for zonally symmetric integration Z1, with a frictional time scale of 6 days. (b) Autocorrelations of the PCs of the first EOFs of three model integrations, each with a different value of the damping time scale (denoted “obs”), and the autocorrelations for three Ornstein-Uhlenbeck (OU) processes with the same damping time scales. The model decorrelates faster than the corresponding OU process, especially when friction is weak.

a zonal asymmetry in the time-mean eddy fluxes), and it is this stationary component that produces the NAO. Momentum fluxes from stationary waves are really the same as the spatially nonuniform eddy fluxes we have parameterized, and that such forcing is responsible for the zonally asymmetric patterns of variability seems consistent with the observational analyses of Limpasuvan and Hartmann (2000).

If this mechanism holds in the real world, then there should be a corresponding phenomena in the Pacific as well as the Atlantic corresponding to the Pacific storm track. Such a “North Pacific Oscillation” (NPO) may well exist [indeed Walker and Bliss (1932) commented on it] although it may not be as noticeable as the NAO because there are many other phenomena occurring in the Pacific, such as El Niño–Southern Oscillation (ENSO) and the Pacific–North American pattern (to

which the NPO may be related). There may well be additional, more subtle differences in the storm tracks between these regions, and we recognize that the differences between the NAO and NPO are unlikely to be fully explained by our proposed mechanism. [A potentially related issue is that there seems to be an observed tendency for the maximum amplitude of the EOFs to be located a little downstream of the storm tracks. We might expect this because momentum fluxes occur primarily in the decaying phase of the baroclinic life cycle, and thus downstream of the center of the storm tracks. Such a mechanism cannot be reproduced in a barotropic model, but nor, in fact, is it a robust feature of simulations with GCMs (CKV). The midwinter suppression of the Pacific storm track is another complicating feature.]

The decorrelation time scale of the NAO and annular modes are observed to be about 10 days, and this is well reproduced by the model, albeit it is partly dependent on the frictional time scale chosen. The eddy forcing itself, even the stationary-eddy forcing, has a much shorter decorrelation time scale (a day or two). The jet integrates this forcing, to produce a redder spectrum, with both the nonlinear dynamics and damping processes providing a limit to the reddening process. The barotropic model does produce variability on long time scales, evidently up to 200 days, although the presence of a seasonal cycle would affect this. Determining whether this long-term variability corresponds to that seen in the observations will require a more detailed study of both model and observations, since the nature of such long-term variability is currently unclear in both. [Feldstein (2000) concludes that the NAO is a Markov process with an  $e$ -folding time scale of about 10 days, whereas Stephenson et al. (2000) note the presence of “long-range dependencies” (a red spectrum) on inter-annual time scales. These may not be contradictory, if the tails in the autocorrelations are nonzero but small.]

It has, of course, been known for some time that rather simple dynamical models and idealized GCMs can reproduce realistic patterns of intraseasonal variability, including annular modes and patterns like the NAO, and that these are associated with variability in the momentum flux. It is also generally accepted that neither stratosphere nor SST anomalies are necessary ingredients for these phenomena. In this paper we have sought to present perhaps the simplest possible model of this as a way of elucidating the dynamics and clarifying the relationship between the NAO and annular modes. In particular, baroclinic effects are modeled by a simple wavemaker that is not related to the strength of the barotropic jet. This suggests that a state dependence of the stirring (that is to say, a feedback from the mean flow to the stirring) is not a crucial ingredient in producing an annular mode or NAO-like structure. However, we do not claim that we have definitively established that such a feedback is not important, and careful studies with both parameterized models and a trustworthy GCM

will be needed before one can definitively pronounce upon this. Furthermore, if we were to construct a model in which the stirring were to depend on the strength of the jet, the eddies might then follow the position of the jet and a longer time scale of variability might thereby be produced.

To conclude, we have presented a simple, dynamically robust mechanism that reproduces some of the important spatial and temporal characteristics of the large-scale variability in the atmosphere. We hope it may be useful as a dynamical basis for more complete models and simulations, and in interpreting the observations.

*Acknowledgments.* We thank Walter Robinson and two anonymous reviewers for their useful comments on an earlier draft, and Isaac Held and Gabriel Lau for helpful discussions. The work was partially supported by NSF under Grant ATM 0337596 and the Hertz Foundation.

## APPENDIX

### Details of Stochastic Forcing

Consider the Ornstein–Uhlenbeck process  $S$  given by the stochastic differential equation

$$\frac{dS}{dt} = -\frac{S}{\tau} + \frac{\sigma\sqrt{2}}{\sqrt{\tau}}\dot{W}, \quad (\text{A.1})$$

with  $S(0) = S_0$ . Suppose that  $S_0$  is chosen from some initial distribution, to be determined below. Here  $S$  is a Gaussian process, and thus wholly characterized by its mean and covariance functions,

$$E[S(t)] = e^{-t/\tau}E[S_0], \quad (\text{A.2})$$

$$\begin{aligned} \text{cov}[S(s), S(t)] &= e^{-(s+t)/\tau} \text{var}(S_0) + \sigma^2 e^{-(t-s)/\tau} \\ &\quad - \sigma^2 e^{-(s+t)/\tau}, \end{aligned} \quad (\text{A.3})$$

where  $s \leq t$ . When  $s, t \gg 0$ , the mean and covariance functions approach

$$E[S(t)] \rightarrow 0, \quad (\text{A.4})$$

$$\text{cov}[S(s), S(t)] \rightarrow \sigma^2 e^{-(t-s)/\tau}, \quad (\text{A.5})$$

regardless of the initial distribution of  $S_0$ . In our model we are interested in the long-term statistical behavior of the system and so lose nothing by taking the initial distribution of  $S_0$  to be the asymptotic distribution,  $N(0, \sigma^2)$ . In this case, (A.2) and (A.3) become (A.4) and (A.5).

We can then simulate  $S(t)$  with the finite difference equation

$$S^i = \sqrt{1 - e^{-2dt/\tau}}\phi^i + e^{-dt/\tau}S^{i-1}, \quad (\text{A.6})$$

where  $dt$  is our time step, and the  $\phi^i$  and  $S^0$  are random variables taken from the Gaussian distribution  $N(0, \sigma^2)$ . The paths  $S^0, S^1, S^2, \dots$  are equivalent to paths of  $S(t)$  sampled at increments of  $dt$ . This follows from the fact

that  $\{S^i\}$ , as a series of sums of Gaussian variables, is a Gaussian process, and thus characterized by its mean and covariance:

$$E[S^i] = 0, \quad (\text{A.7})$$

$$\text{cov}[S^i, S^j] = \sigma^2 e^{-(j-i)d/\tau} \quad (\text{A.8})$$

for  $i \leq j$ , which match the properties of the continuous process above. In our implementation of (A.6), we sample the  $\phi^i$  from a uniform distribution centered about zero, rather than a Gaussian. The modified process is not precisely an Ornstein–Uhlenbeck process: it has the same mean and covariance structure of  $S$ , but slightly different higher moments. It proved advantageous in avoiding occasional large (and unrealistic) spikes in a single wavenumber. For a small time step, the algorithm above reduces to the simpler one presented in Maltrud and Vallis (1991).

#### REFERENCES

- Ambaum, M. H. P., B. J. Hoskins, and D. B. Stephenson, 2001: Arctic Oscillation or North Atlantic Oscillation? *J. Climate*, **14**, 3495–3507.
- Branstator, G., 1992: The maintenance of low-frequency anomalies. *J. Atmos. Sci.*, **49**, 1924–1945.
- Cash, B. A., P. Kushner, and G. K. Vallis, 2002: The structure and composition of the annular modes in an aquaplanet general circulation model. *J. Atmos. Sci.*, **59**, 3399–3414.
- Cohen, J., and K. Saito, 2002: A test of annular modes. *J. Climate*, **15**, 2537–2546.
- DeWeaver, E., and S. Nigam, 2000: Zonal-eddy dynamics of the North Atlantic Oscillation. *J. Climate*, **13**, 3893–3914.
- Feldstein, S. B., 2000: The timescale, power spectra, and climate noise properties of teleconnection patterns. *J. Climate*, **13**, 4430–4440.
- , and S. Lee, 1998: Is the atmospheric zonal index driven by an eddy feedback? *J. Atmos. Sci.*, **55**, 3077–3086.
- Held, I. M., 2000: Lectures. *Proc. Program in Geophysical Fluid Dynamics: The General Circulation of the Atmosphere*, Woods Hole, MA, WHOI. [Available online at: <http://gfd.who.edu/proceedings.html>]
- James, I., and P. M. James, 1992: Spatial structure of ultra-low frequency variability of the flow in a simple atmospheric circulation model. *Quart. J. Roy. Meteor. Soc.*, **118**, 1211–1233.
- Lau, N.-C., 1988: Variability of the observed midlatitude storm tracks in relation to low-frequency changes in the circulation pattern. *J. Atmos. Sci.*, **45**, 2718–2743.
- Lee, S., 1997: Maintenance of multiple jets in a baroclinic flow. *J. Atmos. Sci.*, **54**, 1726–1738.
- Limpasuvan, V., and D. L. Hartmann, 2000: Wave-maintained annular modes of climate variability. *J. Climate*, **13**, 4414–4429.
- Lorenz, D. J., and D. L. Hartmann, 2001: Eddy-zonal flow feedback in the Southern Hemisphere. *J. Atmos. Sci.*, **58**, 3312–3327.
- Maltrud, M. E., and G. K. Vallis, 1991: Energy spectra and coherent structures in forced two-dimensional and beta-plane turbulence. *J. Fluid Mech.*, **228**, 321–342.
- Orlanski, I., 1998: On the poleward deflection of storm tracks. *J. Atmos. Sci.*, **55**, 128–154.
- Rhines, P. B., 1977: The dynamics of unsteady currents. *The Sea*, E. A. Goldberg et al., Eds., Ocean Engineering Science, Vol. 6, Wiley and Sons, 189–318.
- Robinson, W. A., 2000: A baroclinic mechanism for eddy feedback on the zonal index. *J. Atmos. Sci.*, **57**, 415–422.
- Salmon, R., 1980: Baroclinic instability and geostrophic turbulence. *Geophys. Astrophys. Fluid Dyn.*, **10**, 25–52.
- Simmons, A., and B. Hoskins, 1978: The life-cycles of some non-linear baroclinic waves. *J. Atmos. Sci.*, **35**, 414–432.
- Smith, K. S., G. Boccaletti, C. Henning, I. Marinov, F. Tam, I. Held, and G. K. Vallis, 2002: Turbulent diffusion in the geostrophic inverse cascade. *J. Fluid Mech.*, **77**, 34–54.
- Stephenson, D. B., V. Pavan, and R. Bajariu, 2000: Is the North Atlantic Oscillation a random walk? *Int. J. Climatol.*, **20**, 1–18.
- Thompson, D. W. J., and J. M. Wallace, 2000: Annular modes in the extratropical circulation. Part I: Month-to-month variability. *J. Climate*, **13**, 1000–1016.
- Vallis, G. K., and M. E. Maltrud, 1993: Generation of mean flows and jets on a beta plane and over topography. *J. Phys. Oceanogr.*, **23**, 1346–1362.
- Walker, G. T., and E. W. Bliss, 1932: World weather V. *Mem. Roy. Meteor. Soc.*, **4**, 53–83.
- Wallace, J. M., 2000: North Atlantic Oscillation/Annular Mode: Two paradigms—One phenomenon. *Quart. J. Roy. Meteor. Soc.*, **126**, 791–805.
- , and D. S. Gutzler, 1981: Teleconnections in the geopotential height field during the Northern Hemisphere winter. *Mon. Wea. Rev.*, **109**, 784–812.
- Wanner, H., S. Bronnimann, C. Casty, D. Gyalistras, J. Luterbacher, C. Schmutz, D. B. Stephenson, and E. Zoplaki, 2002: North Atlantic Oscillation—Concepts and studies. *Surv. Geophys.*, **22**, 321–381.
- Whitaker, J. S., and P. D. Sardeshmukh, 1998: A linear theory of extratropical eddy statistics. *J. Atmos. Sci.*, **55**, 237–258.